MATERIALS CHEMISTRY
FRONTIERS

Accepted Manuscript

This article can be cited before page numbers have been issued, to do this please use: S. Sharma, T. H. Ho, R. Tian, T. N. Pham, B. K. Mai and T. V. Nguyen, *Mater. Chem. Front.*, 2026, DOI: 10.1039/D6QM00234J.

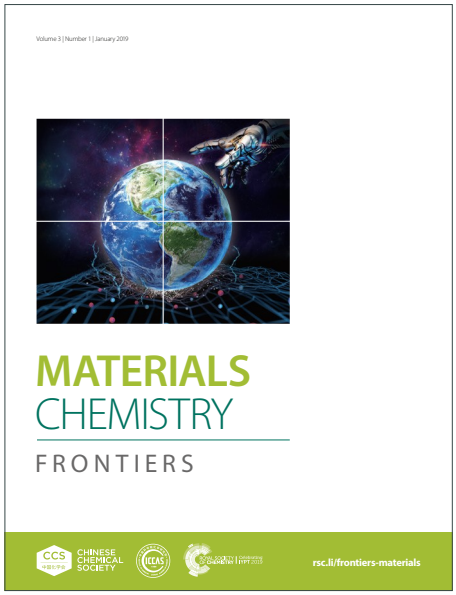

View Article Online
DOI: 10.1039/D6QM00234J

ARTICLE

Dual-State Emissions of Dihydroquinoxaline Derivatives

Sujlesh Sharma,[a] Tuan Hoang Ho,[a] Ruoming Tian,[b] Thanh Nghi Pham,[c] Binh Khanh Mai[d]* and Thanh Vinh Nguyen[a]*

Received 00th January 20xx,
Accepted 00th January 20xx

DOI: 10.1039/x0xx00000x

Abstract: The study of dual-state emissions is an emerging field of research with tremendous potential as DSEgens overcome limitations of two mutually exclusive phenomena of aggregation-caused quenching and aggregation-induced emissions. These materials have versatile applications in optoelectronic devices, bioimaging, chemical sensors, and data encryption. In this study, a new series of dual-state emissive compounds, featuring the dihydroquinoxaline framework is introduced. These derivatives were accessed via facile synthetic routes. By leveraging on specific molecular design strategies such as donor–π–acceptor moieties, partially planar aromatic core with attached phenyl/aryl rings in a twisted molecular conformation, and varying substituents, dual-state emissions were achieved in three dihydroquinoxaline derivatives. These exhibited photoluminescent quantum yields ranging from 47% to 60% in solution, and 42% to 53% in solid states. In contrast, two derivatives showed solid state fluorescence quenching. Single crystal X-ray diffraction analyses reveal key intermolecular hydrogen bonding interactions to the imine nitrogen resulting in fluorescence quenching in these derivatives in the solid state. This study presents the first addition of the dihydroquinoxaline framework to the suite of DSE luminogens.

Keywords: Dual-state emissions, dihydroquinoxalines, luminogens, solid-state emission.

Introduction

Dual-state emissions (DSE) are emissions from materials (DSEgens), in which fluorescence emission is preserved both in solution and solid states.[1] Dual-state emitting (DSE) molecules are fine-tuned, tailored molecular entities with appreciable fluorescence in solution and solid states.[1-3] Thus, a practical consideration for classifying molecules as DSEgens is based on fluorescence quantum yield (Φ_f) ≥5% in both solution and solid states.[3] In this context, solid state typically refers to molecules in their amorphous or (poly-)crystalline condensed state, such as thin films, amorphous powders, crystalline samples, nanoparticles, polymeric matrices, frozen solutions and aggregates in dispersions.[3,4] Emissions arising from different electronic states (eg. singlet and triplet) can also be considered as dual emissive,[5] hence DSEgens are also known as solution and solid state emitters (SSSE) to avoid confusion.[3] This phenomenon was first described by Tang and co-workers in 2015,[6] but this is still an emerging field of research with key design features, underlying photophysical principles and synthesis of DSEgens still being explored.[1-3] Investigations of DSE materials is particularly attractive as they provide several advantages over mutually exclusive phenomena of aggregation-caused quenching (ACQ) and aggregation-induced emission (AIE), which only exhibit fluorescence in dilute solutions, or aggregate forms, respectively.[7-9] Due to their reduced susceptibility to fluorescence quenching,[10,11] DSEgens are versatile molecules with various applications in solution state, for example bioimaging,[12-15] and chemical sensors,[16-18] and in solid state such as optoelectronics,[19-21] and data encryption.[22-24] Another advantage of DSEgens over ACQ- or AIEgens is their concentration-independent photoluminescence, enabling them to function in a range of concentrations.[25]

Emissions from dual states of a single molecule can greatly reduce human effort and time involved in the design, synthesis and optimisation for a number of fluorophores.[2] Key DSE-enabling structural features include twisted structures,[26-30] isolation of fluorophores,[23,31,32] and donor–acceptor architectures,[33-35] while commonly investigated derivatives include tetraphenylethylene (TPE),[36] triphenylamine,[6,37] carbazole,[22,33] organoboron,[38] coumarin,[39,40] single benzene,[41] and excited state intramolecular proton transfer (ESIPT)[42] derivatives.[1] Recently, Voskuhl and co-workers proposed classical and non-classical approaches for the design of DSE molecules.[3] In the classical approach, hybrid molecular structures featuring static cores and rotatable motifs are created. These are a combination of specific AIE and ACQ motifs to obtain emissions in both solution and solid states. For ACQ system, non-radiative decays resulting from intermolecular π–π interactions must be inhibited to allow solid state fluorescence.

[a] School of Chemistry, University of New South Wales, Sydney, Australia
[b] Mark Wainwright Analytical Centre, University of New South Wales, Sydney, Australia
[c] Qui Long Pharmaceutical Co. Ltd., Ho Chi Minh City, Vietnam
[d] Department of Chemistry, University of Pittsburgh, Pennsylvania, United States
* E-mail: t.v.nguyen@unsw.edu.au; binh.mai@pitt.edu

While for AIE, intramolecular motions of functional motifs must be sufficiently restricted while retaining the necessary molecular twist. Thus, planar aromatic core units are combined with moveable, twisted rotors to prevent undesirable excimer formation in the solid state and increase molecular rigidity, allowing restricted motions in the solution state, facilitating fluorescence in both states. Whereas in non-classic approach, a single unified molecule contains planar core and small, flexible groups with subtle rotation and vibration, in a twisted conformation, or intermolecular interactions that prevent deleterious stacking interactions.

Taking inspiration from these design principles, the dihydroquinoxaline framework, which represents a non-classical design approach was chosen for the study of DSE phenomenon. This dihydroquinoxaline molecule is particularly interesting, as it presents a new framework to the existing library of DSEgens, which largely contains common molecular frameworks (*vide supra*). Since appreciable solution and solid state fluorescence[1,2] and Φ_f ≥5%[3] are currently available metrices to classify DSEgens; to the best of our knowledge, comprehensive investigations on the DSE behaviour of dihydroquinoxaline derivatives have not been carried out so far. This work reports a new DSE framework based on the dihydroquinoxaline derivatives and identifies underlying phenomena leading to preserved or quenched fluorescence in dual states. Some dihydroquinoxaline derivatives are known to exhibit strong solution state fluorescence,[43,44] intramolecular charge transfer (ICT),[43,45] AIE,[45] and acid-base sensing[45-48] properties but their DSE properties remain unexplored. Structural features such as sp^2- and sp^3-type (electron acceptor and electron donor) nitrogen in the dihydroquinoxaline core are crucial for its fluorescence properties.[43] Specifically, features such as twisted molecular conformations, donor–π–acceptor (D–π–A) moieties, and asymmetrical, partially planar core of the dihydroquinoxaline framework, may allow molecular rigidity in the solid state, thereby restricting intramolecular motions and facilitating solid state emissions.[1,3] Meanwhile its well-established ICT effect[43,45] will allow efficient solution state fluorescence.

In our group's recent synthesis of 1,2-dihydro-2,2-diaryl-substituted quinoxalines *via* a sequential two-step, one-pot route of quinones, alkynes, and diamines,[49] we observed that some of the dihydroquinoxaline derivatives fluoresced in solution and solid (crystalline and amorphous powder) states. This interesting activity prompted us to investigate a selected number of dihydroquinoxaline derivatives for DSE property. One derivative, **DQ-OH** showed strong solution state fluorescence but quenched solid state emission. The presence of acidic protons on the hydroxyl and amino groups makes this compound susceptible to excited state proton transfer (ESPT) and/or photoacidity processes.[50] To probe if such processes were responsible for the quenched fluorescence behaviour, selected dihydroquinoxaline derivatives were designed, whereby the proton donor and acceptor ability of the motifs in the parent molecule, **DQ-OH** was hindered. By performing *O*- and *N*-methylation, and dehydroxylation, the proton donor hydroxyl group was blocked (**DQ-OMe** and **DQ-OMe-NMe**), weak proton donor amino nitrogen was blocked (**DQ-NMe** and **DQ-OMe-NMe**), and the proton donor ability completely removed (**DQ** and **DQ-NMe**) (See Figure 1 and SI - Scheme 1). While some DSEgens have also shown emission in aggregate form,[13] the focus of this investigation is on dual emissions arising from isolated (dilute solution) and bulk solid (crystalline and amorphous powder) states.[3,4]

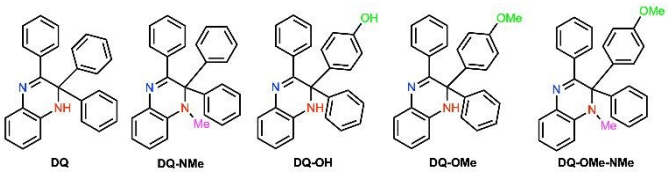

Figure 1. Selected dihydroquinoxaline derivatives being investigated in this study.

Results and Discussion

Synthesis of dihydroquinoxaline derivatives

Compound **DQ** was prepared according to slightly modified procedure described by Son *et al.*[43] Arylation of 2,3-diphenyl quinoxaline with phenyl bromide and *n*-butyllithium yielded **DQ** (see Scheme 1 (a)).[43] Compound **DQ-NMe** was prepared from compound **DQ** following the procedure described by our group earlier.[49] Methylation of **DQ** with methyl iodide, using sodium hydroxide furnished **DQ-NMe**.[49] The crude products were purified using flash column chromatography using eluent mixtures of *n*-hexane and ethyl acetate. Compounds **DQ** and **DQ-NMe** were obtained as light-yellow solids in 65% and 70% yields, respectively (see SI Figure 1).

Synthesis of compound **DQ-OH** commenced with a reaction between 1,4-benzoquinone, 1,2-diphenylethyne and 1,2-diaminobenzene using blue LED reactor (see Scheme 1 (b)).[49] Methylation of **DQ-OH** using varying equivalents of methyl iodide and sodium hydroxide furnished crude **DQ-OMe** and **DQ-OMe-NMe**.[49] The crude products were purified in the similar manner as **DQ** and **DQ-NMe**, to furnish compounds **DQ-OH** as light yellow solid in 95% yield, **DQ-OMe** as yellow solid in 91% yield, and **DQ-OMe-NMe** as intense yellow solid in 87% yield (see SI Figure 1). Compounds **DQ**, **DQ-NMe**, **DQ-OH** and **DQ-OMe** were classed as crystalline powder, while **DQ-OMe-NMe** as amorphous powder based on their powder X-ray diffraction (PXRD) patterns (see SI - Figures 21 and 22).

View Article Online
DOI: 10.1039/D5QM00237J

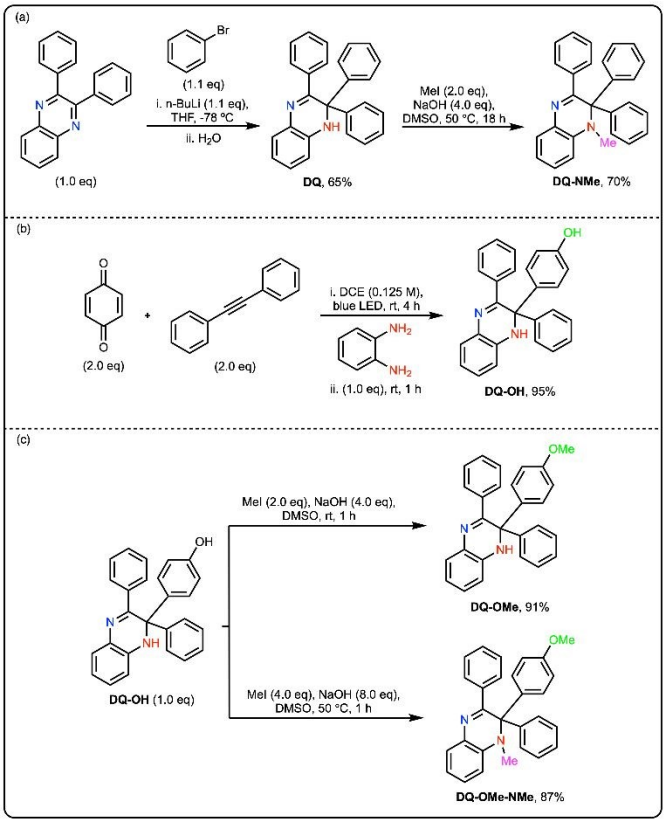

Scheme 1. Synthesis of dihydroquinoxaline derivatives: (a) **DQ** and **DQ-NMe**, (b) **DQ-OH**, and (c) **DQ-OMe** and **DQ-OMe-NMe**.

Photophysical properties of dihydroquinoxaline derivatives in solution and solid states

The photophysical properties of the dihydroquinoxaline derivatives were studied in their solution (25 µM in DCM) and bulk solid states (see Table 1). Solution state UV-vis absorption spectra showed strong absorption bands between 250 to 270 nm, attributed to π–π* transition, slight shoulder *ca*. 300 nm for compounds **DQ**, **DQ-OH** and **DQ-OMe**, and a weak absorption band around 375 to 392 for all compounds (see SI - Figure 2). This red-shifted band is attributed to n–π* transition and could be due to the charge transfer band resulting from electron-donating amine and electron-accepting imine groups. Compounds **DQ**, **DQ-OH** and **DQ-OMe** had charge transfer band λ_{abs} at 375 nm, while compounds **DQ-NMe** and **DQ-OMe-NMe** had charge transfer band λ_{abs} at 392 nm due to methyl substituent on the amino nitrogen. Dilute solutions of all the dihydroquinoxaline derivatives exhibited strong fluorescence emission in the greenish-yellow region upon irradiation under long UV light (see Figure 2(c)).

The fluorescence emission λ_{em} for all the compounds were almost the same, with λ_{em} 525 nm for **DQ**, **DQ-OH** and **DQ-OMe**, and λ_{em} 532 nm for **DQ-NMe** and **DQ-OMe-NMe** (see Figure 2 (a)). All the compounds had large Stokes shift (see Table 1), which is typical for compounds showing ICT effect. The CIE 1931 chromaticity plot showed two distinct spots in the green-yellow region for these two sets of compounds (see SI - Figure 4 (a)). Compound **DQ-OMe-NMe** exhibited the highest fluorescence quantum yield, Φ_f = 60.2%, followed by **DQ** (Φ_f = 59.6%), **DQ-OH** (Φ_f = 54.1%), **DQ-OMe** (Φ_f = 51.9%), while **DQ-NMe** had the lowest quantum yield (Φ_f = 47.5%) (see Table 1). High quantum yields could be due to the ICT effects in these molecules.[43] All the compounds showed average fluorescence lifetime (τ_{ave}) ranging from 7.00 ns to 11.5 ns. Compound **DQ-OMe-NMe** had the lowest τ_{ave} of 7.00 ns, while compound **DQ** had the highest τ_{ave} of 11.5 ns (see Table 1). This is consistent with compound **DQ-OMe-NMe**, which has the highest Φ_f also has the highest radiative decay constant (k_r = 0.086 ns^{-1}). Compound **DQ-NMe** has the lowest Φ_f and has the highest non-radiative decay constant (k_{nr} = 0.063 ns^{-1}), compared to other compounds (see Table 1). A high radiative decay constant and low non-radiative decay constant indicate an efficient system and *vice-versa*.[29]

The absorption spectra for solid state samples showed broad absorption bands ranging from 379 to 428 nm. All compounds are light-yellow, except for **DQ-OMe-NMe**, which is intense yellow in colour (see SI - Figure 3). Thus, compound **DQ-OMe-NMe** showed the most bathochromic shifted λ_{ab} at 428 nm, followed by compounds **DQ-NMe** (λ_{ab} = 414 nm), **DQ-OMe** (λ_{ab} = 413 nm), **DQ** (λ_{ab} = 398 nm), and **DQ-OH** (λ_{ab} = 379 nm) (see Table 1). The fluorescence emission spectrum of compound **DQ-OMe-NMe** showed the most red-shifted emission wavelength (λ_{em} = 523 nm), followed by compounds **DQ-OH** (λ_{em} = 512 nm), **DQ** (λ_{em} = 508 nm), and **DQ-OMe** (λ_{em} = 495 nm), **DQ-NMe** (λ_{em} = 486 nm) (see Table 1 and Figure 2 (b)). The CIE 1931 chromaticity plot showed five distinct spots in the blue to yellow region for these compounds (see SI - Figure 4 (b)), which aligned to emissions observed from the solid samples under long-UV irradiation (see Figure 2 (d)). The Stokes shift for compounds in solid state was smaller than those obtained for solution samples (see Table 1). Unlike the solution samples, the solid samples showed quantum yields ranging from very low to high (Φ_f = 1.7% – 52.9%). This behaviour was intriguing. Compound **DQ-OMe** had the highest Φ_f = 52.9%, which was very similar to the solution sample (Φ_f = 51.9%). Compound **DQ-OMe-NMe** had Φ_f = 52.1%, which was slightly less than that of the solution sample (Φ_f = 60.2%). Compound **DQ** had Φ_f of 41.7%, which was much lower than that of the solution sample (Φ_f = 59.6%). The fluorescence quantum yields of compounds **DQ-NMe** (Φ_f = 5.1%) and **DQ-OH** (Φ_f = 1.7%) were very low, and significantly lower than those of corresponding solution samples (Φ_f = 47.4% and 54.1%), respectively (see Table 1).

View Article Online
DOI: 10.1039/D6QM00234J

Table 1. Table showing photophysical properties of dihydroquinoxaline derivatives in solution and solid states. All the emission measurements were made with λ_{ex} values.

Property	Compounds in Solution State					Compounds in Solid State				
	DQ	**DQ-NMe**	**DQ-OH**	**DQ-OMe**	**DQ-OMe-NMe**	**DQ**	**DQ-NMe**	**DQ-OH**	**DQ-OMe**	**DQ-OMe-NMe**
λ_{abs} (nm)	375	392	375	375	392	398	414	379	413	428
λ_{ex} (nm)	375	392	375	375	392	440	428	433	423	450
λ_{em} (nm)	525	532	525	525	532	508	486	512	495	523
Φ_f (%)	59.6	47.4	54.1	51.9	60.2	41.6	5.1	1.7	52.9	52.1
τ_{ave} (ns)	11.5	8.41	10.9	11.3	7.00	8.00	1.10	0.63	7.15	9.78
k_r (ns^{-1})	0.052	0.056	0.047	0.046	0.086	0.052	0.047	0.027	0.074	0.053
k_{nr} (ns^{-1})	0.035	0.063	0.042	0.043	0.057	0.073	0.862	1.560	0.066	0.049
Stokes shift (cm^{-1})	7619	6713	7619	7619	6713	3042	2788	3563	3439	3102

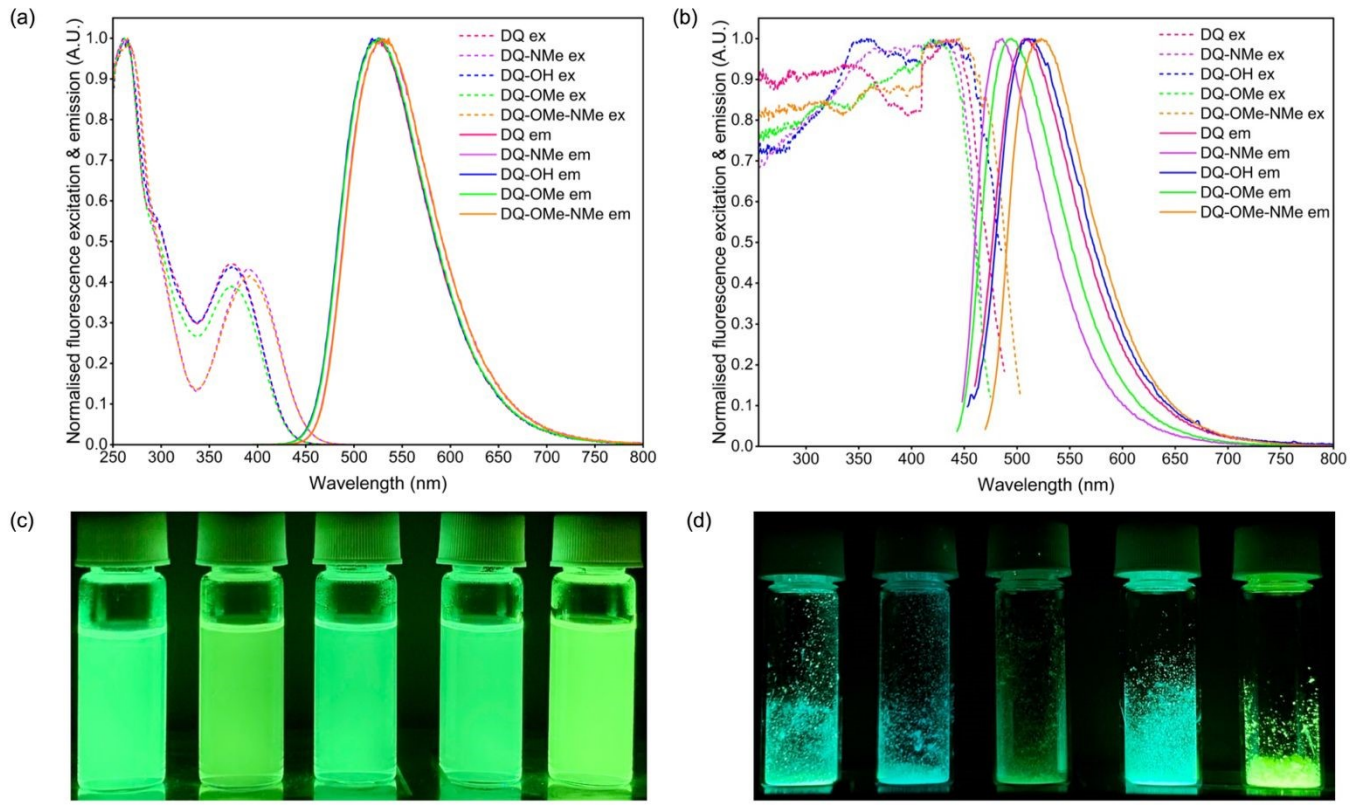

Figure 2. Normalised fluorescence emission spectra of dihydroquinoxaline derivatives in solution (25 µM in DCM) (a) and solid state (b). Fluorescence emissions of derivatives **DQ**, **DQ-NMe**, **DQ-OH**, **DQ-OMe** and **DQ-OMe-NMe** (L-R) under long UV irradiation (365 nm) for solution (c) and solid states (d).

Compounds that showed high quantum yields also had higher τ_{ave} values compared to those that had low quantum yields. Compounds **DQ-OMe**, **DQ-OMe-NMe** and **DQ** had τ_{ave} of 7.15 ns, 9.78 ns and 8.00 ns, respectively. Compound **DQ-OMe** had the highest k_r = 0.074 ns^{-1}, being most efficient emitter. Compounds **DQ-NMe** and **DQ-OH** had τ_{ave} of 1.10 ns and 0.63 ns. Compound **DQ-OH** had the highest non-radiative decay constant, k_{nr} = 1.560 ns^{-1}, indicating the most inefficient emitter. This was followed by the k_{nr} of **DQ-NMe** (0.862 ns^{-1}) (see Table 1). The high non-radiative decay constant suggests the presence of mechanisms contributing to fluorescence quenching for compounds **DQ-NMe** and **DQ-OH** in the solid state. Establishing clear correlations between substituents on dihydroquinoxaline derivatives and their emission wavelengths remains challenging. Compound **DQ-OMe-NMe**, bearing two electron-donating *N*-methyl and methoxy substituents, exhibited the most bathochromic shift. In contrast, **DQ-NMe** and **DQ-OMe**, with only one of these substituents, showed the most pronounced hypsochromic shifts. While both **DQ** and **DQ-OH** displayed nearly identical emission wavelengths despite the presence of a hydroxyl group in the latter. Compounds **DQ-OMe**, **DQ-OMe-NMe**, and **DQ**, which retain relatively high quantum yields in both solution and solid states, were classified as dual-state emitters.[1,3] Compound **DQ-NMe** has Φ_f =5.1%, which could also be a DSEgen but as it has highly reduced solid state Φ_f similar to that of **DQ-OH**, they both show aggregation-caused emission weakener (ACEW) effect.[3] This could be likely due to aggregation-caused quenching, internal conversion, and,

Journal Name ARTICLE

View Article Online
DOI: 10.1039/D5QM00374J

for **DQ-OH**, deactivating hydrogen bonding.[52] The effects of aggregation on the emission properties of all the dihydroquinoxaline derivatives were carried out using THF/water mixtures. All the derivatives showed gradual bathochromic shifts as the f_{water} (vol%) increased to *ca*. 70%, suggesting ICT effect with increasing solvent polarity (see SI - Figures 7–12).[45] Derivatives **DQ**, **DQ-NMe**, **DQ-OMe**, **DQ-OMe-NMe** did not show typical AIE or ACQ behaviour upon aggregation, **DQ-OH** showed ACQ properties.[8] To further elucidate all these behaviours, single-crystal X-ray diffraction (SC-XRD) analyses were conducted (*vide infra*).

To investigate ICT phenomenon in these derivatives, compound **DQ-OH** was selected and 25 µM solution were prepared in various non-polar, polar, polar protic and aprotic solvents. The UV-vis absorption spectra showed a charge transfer band *ca*. 375 nm for solutions prepared in hexane, toluene and DCM, while solutions prepared in THF, EtOH and DMSO showed a bathochromic shift with λ_{abs} 386 – 392 nm. The fluorescence emission spectra for non-polar solvents hexane and toluene, ($E_T(30)$ values, which is a measure of the microscopic solvent polarity, of *ca*. 31 – 34)[53,54] had a hypsochromic-shifted emission (λ_{em} = 507 and 511 nm), emission of λ_{em} 530 and 525 nm for THF and DCM ($E_T(30)$ *ca*. 37 – 41) and red-shifted emissions of λ_{em} of 554 and 564 nm with DMSO and EtOH ($E_T(30)$ *ca*. 45 – 52), respectively (Figure 3).

Figure 3. Normalised fluorescence emission spectra of **DQ-OH** in various solvents (25 µM)

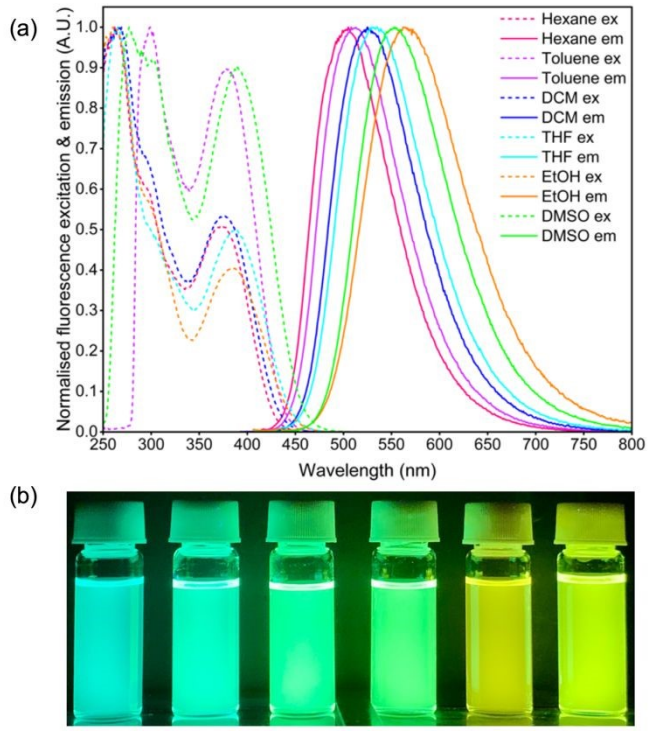

(a). Samples were excited as follows: hexane (λ_{ex} = 372 nm), toluene (λ_{ex} = 378 nm), DCM (λ_{ex} = 375 nm), THF (λ_{ex} = 388 nm), EtOH (λ_{ex} = 386 nm) and DMSO (λ_{ex} = 392 nm). Solutions of **DQ-OH** in various solvents (L-R): hexane, toluene, DCM, THF, EtOH, and DMSO (25 µM) under long UV irradiation (365 nm) (b).

Moderate to high Stokes shift were obtained for the different solutions ranging from 7001 cm^{-1} (131 nm for hexane) to 8176 cm^{-1} (178 nm) for EtOH (see SI - Table 2). Hexane solution gave the shortest τ_{ave} of 5.28 nm, while toluene and EtOH solutions gave slightly higher values of 7.31 and 8.75 nm, and THF, DCM and DMSO solutions gave high τ_{ave} values of 11.99, 12.48 and 15.36 ns, respectively. A linear relationship was seen between the Stokes shift and emission maxima with the $E_T(30)$ values (see SI - Figures 5 and 6), confirming positive solvatochromism, which supports the existence of ICT effects.[53] Bathochromic shifts with DMSO and EtOH could be attributed to stabilisation of charge-separated excited state by polar solvents, which lowers the energy of this state and leads to red-shifted emission.[51,55] Highest τ_{ave} value for DMSO indicates enhanced stabilisation of the excited state, resulting in slower radiative decay. While EtOH exhibited the most red-shifted emission maximum (λ_{em}), its moderate τ_{ave} value may be explained by strong hydrogen bonding (HB) interactions,[56] which favour non-radiative decay pathways via internal conversion, by providing an efficient vibrational mode for excited-state deactivation.[52] The ICT effects arising from the asymmetrical molecular structure with D–π–A system and electron rich phenyl rings[43] may enhance radiative decay, giving high quantum yield for these derivatives. To confirm the existence of the ESPT phenomenon,[50,57] pH-dependent studies were carried out for **DQ-OH** using hydrogen bond (HB) acceptor and donor (EtOH), HB acceptor (DMSO) and HB neutral (DCM) solvents and an organic base DBU, and acid, TFA. Treatment of a 25 µM solution of **DQ-OH** with up to 100 equivalents of DBU and TFA may deprotonate the hydroxyl proton and protonate the imine group, respectively (see Scheme 2).

Scheme 2. Deprotonation and protonation of **DQ-OH** with DBU and TFA in solution (25 µM).

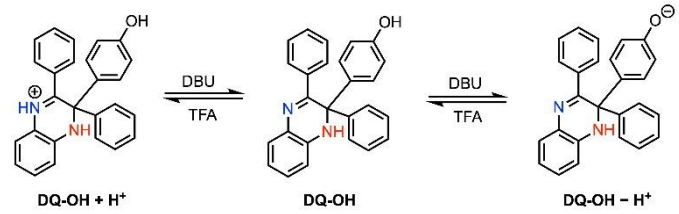

Treatment with DBU caused an increase in band between 250 and 270 nm in the UV-vis absorption spectra for all the solvents (see Figure 4, a-c). This could be due to change in the electronic states arising from the phenoxide ion. As expected, no change was seen in the charge transfer band upon DBU addition. Treatment with TFA, red-shifted the charge transfer band and decreased the intensity for band at 250 and 270 nm in DCM and EtOH (Figure 4, a and b). TFA did not have any effect in DMSO (Figure 4, c). Bathochromic shifts seen in the charge transfer band may result from iminium ion, which seems to be stabilised in DCM and EtOH. Slight red-shifting and increase in intensity was seen for the shoulder band at *ca*. 300 nm. These changes are most pronounced in DCM, followed by EtOH and DMSO. Irradiation of fresh samples with long UV light (365 nm), caused similar changes but with less intensity compared to TFA treatment. since DCM does not participate in hydrogen bonding, the hydroxyl and imine groups are most susceptible to proton transfer. While in EtOH, these groups may be hydrogen bonded with EtOH for some molecules, hence less prone to

View Article Online
DOI: 10.1039/D6QM00234J

proton transfer. In DMSO, since most hydroxyl protons may be hydrogen bonded to DMSO, and possibly TFA also protonating DMSO instead of the imine, minimal proton transfer may take place. This was further verified as the most fluorescence quenching was seen in DCM with both acid and base treatment, followed by moderate quenching in EtOH and almost no quenching seen for DMSO (see Figure 4, d–f). This pH-dependent study confirmed that the quenching could be attributed to proton transfer. Concentration-dependent studies were carried out in DCM to further investigate fluorescence quenching in **DQ-OH**. Figure 14 in SI shows that as the concentration of DCM solution increased, the intensity of absorption bands increased. As the concentration increased from 25 µM to 625 µM, fluorescence intensity gradually increased and decreased thereafter, suggesting that **DQ-OH** is emissive in both dilute solution and concentrated solutions up to 2.5 mM. Within this range, **DQ-OH** may show a combination of sufficient rotation and twisting, enabling fluorescence at both dilute and concentrated solutions. Further increase in concentration, may impart solid like characteristics to the molecules, hence fluorescence quenching is seen after 2.5 mM.

Figure 4. UV-vis absorption (top) and fluorescence emission (bottom) spectra of **DQ-OH** solution (black), **DQ-OH** solutions upon treatment with 100 equivalence of DBU (red) and TFA (blue), and irradiation at 365 nm for 30 min (green). All solutions (25 µM) are prepared in DCM (column 1), EtOH (column 2) and DMSO (column 3). Different colours and sizes

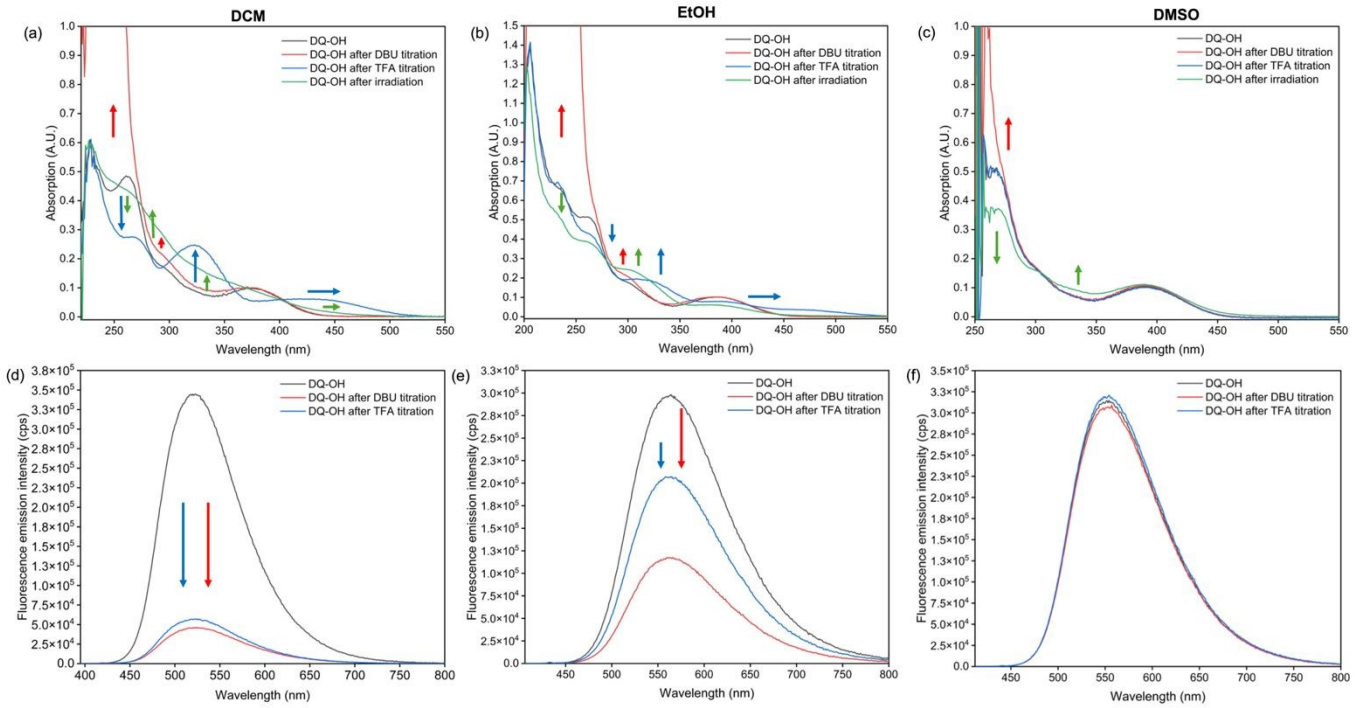

of arrows represent increase/decrease/shift in absorption bands and emission intensity with respect to various treatments.

XRD Analyses

Single crystal XRD (SC-XRD) analyses revealed that the dihydroquinoxaline framework, consisting of a benzene ring fused to a non-planar dihydropyrazine unit with three phenyl or aryl groups in a twisted conformation, render these molecules non-planar (see Figure 5 (column 1) and SI - Table 3). The torsion angle between conjugated aromatic rings in the fluorophore is critical for DSE property[1] and are influenced by substituents on the phenyl rings and intermolecular interactions in the crystal lattice.[26] Compounds **DQ**, **DQ-OH** and **DQ-OMe** have comparable torsion angles, while the torsion angles in compound **DQ-NMe** differ significantly due to the methyl group on the nitrogen atom, inducing greater dihedral angles for rings 1 and 2, and further twisting of ring 3 (see SI Table 3). Large torsion angles are important as they twist the molecular structure in the solid state, inhibiting close packing and preventing deleterious π···π stacking interactions, thus promoting radiative decay processes.[3]

Substituents on the amino nitrogen or phenyl ring further influence molecular orientation, packing and specific intermolecular interactions, accounting for three distinct packing arrangements. Compounds **DQ** and **DQ-OH** have face-to-edge packing with nearly perpendicular aromatic rings, revealing a Herringbone stacking pattern along the *a* axis (see SI Figure 17 and 19).[58] This arrangement likely arises from the molecule's twisted conformation and is stabilised by several short-range CH···π (2.719 – 3.087 Å) interactions (see Figure 5 (b and h) and SI - Table 5). Compound **DQ-NMe** adopts a spiral ladder like arrangement, likely driven by the methyl group, to minimise steric and electronic repulsion (see SI - Figure 18). In compound **DQ-OMe**, two molecules form dimeric head-to-tail arrangement, with the methoxy oriented toward each other along the *b* axis (see SI - Figure 20).

View Article Online
DOI: 10.1039/D6QM00234J

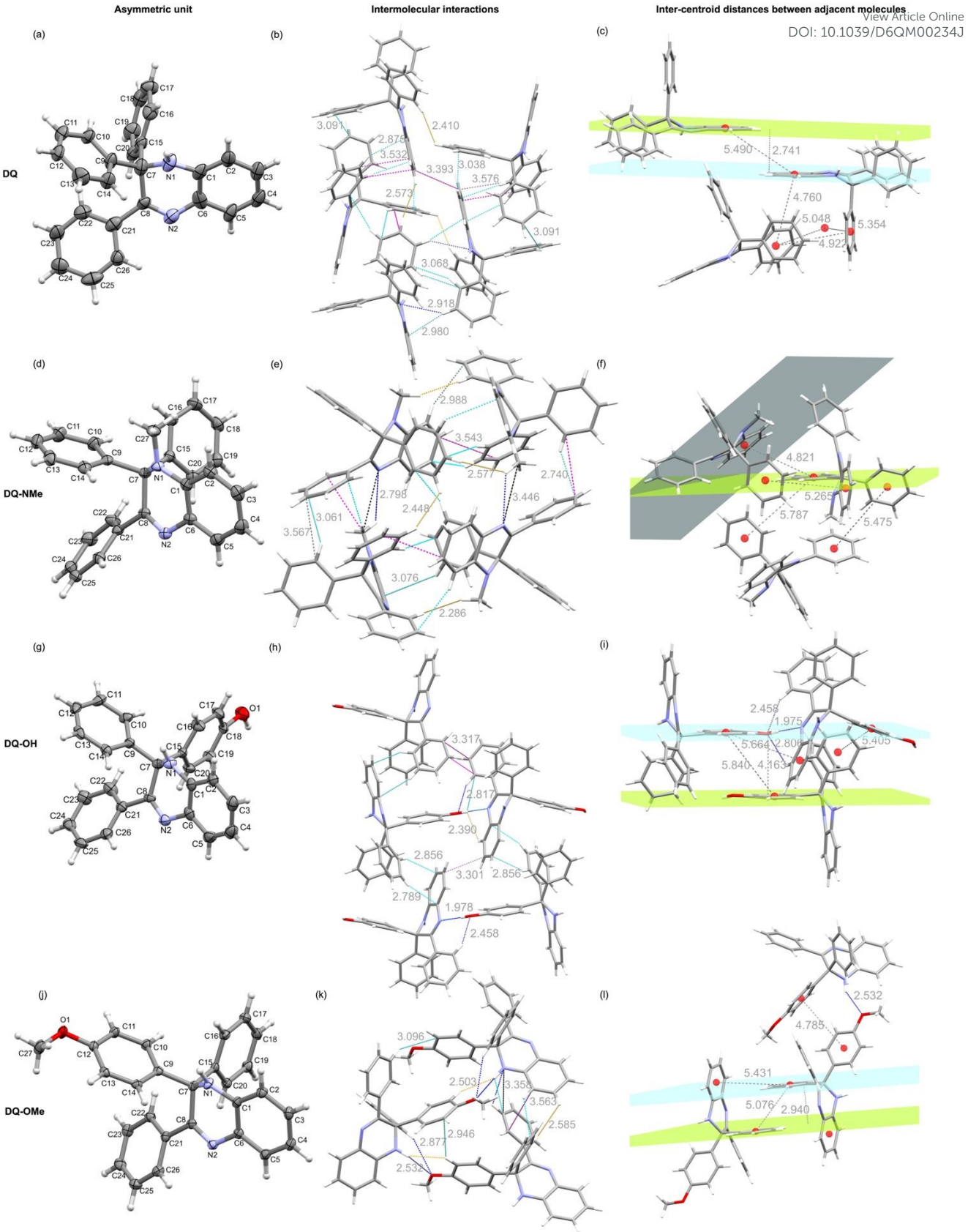

Figure 5. Single crystal structure analyses of dihydroquinoxaline derivatives. Column 1: asymmetric units; crystal structures for all showing 50% probability ellipsoids for all non-hydrogen atoms, except for **DQ**, which is showing 40% probability. Column 2: selected intermolecular interactions (in Å) in the crystal lattice. Interactions are coloured as follows: i) dark blue (hydrogen bonds): CH···NH, OH/CH_3···N, CH···O, and NH···O); ii) cyan: CH···π; iii) magenta: π···π or π···CH_3; iv) yellow: CH···HC or CH···HN or CH···HO or CH···H_3C; and v) black: C···N/NH. Column 3: distances between the centroids in the phenyl rings (in Å) between mean planes of the phenyl rings (grey/blue and green).

A distinct difference between solid state emitters (**DQ** and **DQ-OMe**), and weak emitters (**DQ-OH** and **DQ-NMe**) lies in the type of nitrogen atom engaged in the intermolecular HB interactions (see Figure 5 (column 2) and SI - Figure 16). In **DQ** and **DQ-OMe**, the sp^3 amino nitrogen functions as both HB donor and acceptor, whereas in **DQ-NMe** and **DQ-OH**, the sp^2 imine nitrogen behaves as HB acceptor only. Furthermore, compounds **DQ** and **DQ-NMe** only possess weak HB interactions, while the hydroxyl and methoxy substituents in **DQ-OH** and **DQ-OMe** promote strong HB interactions.[59] Compound **DQ** has CH···NH (2.918 Å) HB interaction.

The orientation of the methyl group in compound **DQ-NMe** facilitates weak HB interactions from the methyl protons to the imine nitrogen (CH_3···N (2.798 Å)). Compound **DQ-OH** has strong (OH···N, 1.978 Å) and weak (CH···O, 2.458 Å) HB interactions. The orientation of the methoxy group in **DQ-OMe** allows strong (NH···O, 2.790 Å), and weak CH···N (2.877 Å) or CH···O (2.532 Å) HB interactions, consistent with distances for HB interactions for ether groups.[59,60] Intermolecular HB interactions seen in **DQ-NMe** and **DQ-OH** enhance the deactivation of the excited state through internal conversion, promoting efficient non-radiative decay processes.[52]

In the crystal lattice of the dihydroquinoxaline derivatives, key short-range interactions include π···π interactions (3.301 – 3.569 Å), consistent with effective intermolecular charge transfer and potentially explaining the slightly reduced quantum yield in solid state for compounds **DQ** and **DQ-OMe**. Additional stabilising interactions such as CH···π (2.719 – 3.096 Å), CH···HC/HN/HO/H_3C (2.074 – 2.585 Å), and C···N/NH (3.358 – 3.446 Å) were also observed (see Figure 5 (column 2) and SI - Table 5).

In the dihydroquinoxaline derivatives, molecular arrangements, intermolecular distances and HB interactions strongly influence solid state fluorescence. In compounds **DQ** and **DQ-OH**, aromatic rings adopt a face-to-edge arrangement, while the molecules exist co-facially on parallel planes with slip angles of 30.37° and 48.75°, and perpendicular distances between two parallel planes of 2.777 Å and 4.163 Å, respectively (see Figure 5 (c and i) and SI - Table 4). Large inter-centroid distances (4.760 – 5.840 Å) prevent effective π···π interactions to occur. While both **DQ** and **DQ-OH** have similar molecular arrangements, differences in their HB interactions render **DQ** as an efficient solid state emitter unlike **DQ-OH**. Compound **DQ-NMe** has slanted face-to-face arrangement of the phenyl rings and possesses large inter-centroid distances (4.821 – 5.787 Å) (see Figure 5 (f) and SI - Table 4). In solid state, the unfavourable HB interactions and partial charge transfer through π···π interactions (3.301 – 3.567 Å) seem to be the main cause of fluorescence quenching. Compound **DQ-OMe** has two phenyl rings in co-facial, parallel arrangement with a slip angle of 41.01° and centroid-to-centroid distance of 5.076 Å (see Figure 5 (l) and SI Table 4). The two aryl groups are arranged head-to-tail at an angle of 96.32° and inter-centroid distance of 4.785 Å. A perpendicular distance between the parallel planes is 2.940 Å, and other centroid-to-centroid distances include 5.431 Å. Large intermolecular centroid distances prevent close molecular packing and π···π stacking interactions. A combination of loose molecular packing, rigid twisted conformations and either favourable or unfavourable hydrogen bonding interactions either preserve or quench fluorescence in solid state dihydroquinoxaline derivatives.

To provide theoretical support for the photophysical behaviour of the dihydroquinoxaline derivatives, TD-DFT calculations were performed at the (TD)ωB97X-D/def2-TZVPP//(TD)CAM-B3LYP-def2-SVP level (see the ESI for further details). Efficient dual-state emitters are generally associated with relatively large oscillator strengths and limited structural reorganisation between the ground and excited states.[61] All five compounds exhibit oscillator strengths of 0.197–0.212 and RMSD values of 0.727–1.017 Å, consistent with efficient fluorescence (see page S50 in the ESI). The calculations further indicate that the $S_0 \rightarrow S_1$ transition is dominated by a HOMO→LUMO excitation with charge transfer from the amino/aryl donor region to the imine-containing acceptor fragment. Notably, the calculated LUMO is localized on the imine nitrogen in all derivatives. Single-crystal X-ray diffraction analysis revealed intermolecular interactions involving this imine nitrogen in **DQ-NMe** and **DQ-OH**, the two compounds that exhibit strongly quenched solid-state fluorescence, suggesting that these interactions contribute to enhanced non-radiative decay in the solid state. Overall, the calculations provide a theoretical rationale for both the dual-state emission of **DQ**, **DQ-OMe**, and **DQ-OMe-NMe** and the solid-state fluorescence quenching of **DQ-NMe** and **DQ-OH**.

Conclusions

In conclusion, judicious choice of molecular design features such as D–π–A moieties, partially planar core with aromatic rings in a twisted molecular conformation and appropriate substituents can engender simple dihydroquinoxaline derivatives as DSEgens. The synergy of molecular features, along with key intermolecular hydrogen bonding interactions can be useful in preserving or quenching fluorescence in solid state. This study introduced a new framework, together with key photophysical and SC-XRD insights for the design and synthesis of future DSE luminogens with very good PLQY in dual states. Herein, all compounds showed very good solution state photoluminescence behaviour with PLQY ranging from 47% to 60%. Three derivatives (**DQ**, **DQ-OMe** and **DQ-OMe-NMe**) showed very good PLQY (42% to 53%) in solid state. The dihydroquinoxaline framework can be enhanced to develop DSE luminophores with targeted photoluminescent properties and enhanced efficiency for various applications such as chemo-sensors and biological imaging. This study presents the first introduction of the dihydroquinoxaline framework to the suite of DSE luminogens.[1,3,14-16,18,21,24,25,40-42,46]

Author contributions

Compound synthesis: THH and SS. Photophysical studies: SS and THH. XRD data collection and analyses: SS and RT. Instrumentation: TNP. Computational studies: BKM. Project design and supervision: TVN. Writing – original draft: SS, BKM. Writing – review & editing: TVN.

Conflicts of interest

The authors declare that they have no competing interests.

Data availability

All data are available in the main text or the ESI. All crystal structures have been deposited in the CCDC in the cif format under 2463720, 2463716, 2463715 and 2463714 for **DQ**, **DQ-NMe**, **DQ-OH** and **DQ-OMe**, respectively. References cited in the ESI[43,54,62-67] have been included in Notes and References section.

Acknowledgements

The authors thank the Australian Research Council (grant DP260100065 to TVN) and UNSW Faculty of Science for financial support.

Notes and references

1. J. L. Belmonte-Vázquez, Y. A. Amador-Sánchez, L. A. Rodríguez-Cortés and B. Rodríguez-Molina, Dual-state emission (DSE) in organic fluorophores: Design and applications, *Chem. Mater.*, 2021, **33**, 7160-7184.
2. L. A. Rodríguez-Cortés, A. Navarro-Huerta and B. Rodríguez-Molina, One molecule to light it all: The era of dual-state emission, *Matter*, 2021, **4**, 2622-2624.
3. A. Huber, J. Dubbert, T. D. Scherz and J. Voskuhl, Design concepts for solution and solid-state emitters – a modern viewpoint on classical and non-classical approaches, *Chem. Eur. J.*, 2023, **29**, 202202481.
4. J. Gierschner, J. Shi, B. Milián-Medina, D. Roca-Sanjuán, S. Varghese and S. Park, Luminescence in crystalline organic materials: From molecules to molecular solids, *Adv. Opt. Mater.*, 2021, **9**, 2002251.
5. S. K. Behera, S. Y. Park and J. Gierschner, Dual emission: Classes, mechanisms, and conditions, *Angew. Chem., Int. Ed.* , 2021, **60**, 22624-22638.
6. G. Chen, W. Li, T. Zhou, Q. Peng, D. Zhai, H. Li, W. Z. Yuan, Y. Zhang and B. Z. Tang, Conjugation-induced rigidity in twisting molecules: Filling the gap between aggregation-caused quenching and aggregation-induced emission, *Adv. Mater.*, 2015, **27**, 4496-4501.
7. J. Mei, N. L. C. Leung, R. T. K. Kwok, J. W. Y. Lam and B. Z. Tang, Aggregation-induced emission: Together we shine, united we soar!, *Chem. Rev.*, 2015, **115**, 11718-11940.
8. Z. Zhao, H. Zhang, J. W. Y. Lam and B. Z. Tang, Aggregation-induced emission: New vistas at the aggregate level, *Angew. Chem., Int. Ed.*, 2020, **59**, 9888-9907.
9. M. K. Bera, P. Pal and S. Malik, Solid-state emissive organic chromophores: design, strategy and building blocks, *J. Mater. Chem. C*, 2020, **8**, 788-802.
10. B. Prusti, S. Tripathi, P. Sivasakthi, P. K. Samanta and M. Chakravarty, Solution and Solid-State Emissive Organophosphonates with High-Contrast Reversible Mechanofluorochromism: Beyond the Classical Frameworks, *ACS Appl. Opt. Mater.*, 2023, **1**, 889-897.
11. L. Zou, S. Guo, H. Lv, F. Chen, L. Wei, Y. Gong, Y. Liu and C. Wei, Molecular design for organic luminogens with efficient emission in solution and solid-state, *Dyes Pigm.*, 2022, **198**, 109958.
12. S. Bhuin, P. Chakraborty, P. Sivasakthi, P. K. Samanta and M. Chakravarty, Double-site twisted D-π-D′ conjugates with versatile photophysical facets for diverse optical applications and wash-free bioimaging of cancer cells, *ACS Appl. Opt. Mater.*, 2023, **1**, 1289-1300.
13. S. Bhuin, P. Sharma, P. Chakraborty, O. P. Kulkarni and M. Chakravarty, Solid-state emitting twisted π-conjugate as AIE-active DSE-gen: in vitro anticancer properties against FaDu and 4T1 with biocompatibility and bioimaging, *J. Mater. Chem. B*, 2023, **11**, 188-203.
14. Y. Liu, J. Zhang, S. Jiang, S. Zhang and G. Feng, Dual-State Emission Fe2+-Activation Probe Capable of High-Contrast Brain Imaging Reveals an Age-Dependent Accumulation of Fe2+ in the Brain, *Anal. Chem.*, 2025, **97**, 26668-26676.
15. L. Wang, Y. Sun, C. Yu, W. Ma, Y. Shang, L. Ding, T. Wang, X. Guo, J. Zhang, Y. Li, E. Hao, G.-W. Wang and L. Jiao, Electron-donating boronic salicylhydrazones as dual-state emissive fluorophores for lipid droplet imaging, *Org. Lett.*, 2025, **27**, 8551-8556.
16. B. Prusti, S. Tripathi, A. Jain and M. Chakravarty, Concentration-guided visual detection of multiphase aliphatic biogenic amines through amine–phenol recognition using a dual-state emitter, *ACS Appl. Mater. Interfaces*, 2023, **15**, 16492-16504.
17. D. Xi, Y. Xu, R. Xu, Z. Wang, D. Liu, Q. Shen, L. Yue, D. Dang and L. Meng, A facilely synthesized dual-state emission platform for picric acid detection and latent fingerprint visualization, *Chem. Eur. J.*, 2020, **26**, 2741-2748.
18. P. A. Chaudhran, S. Y. Mastoli, A. Dey, S. A. Saraf and A. Sharma, Dual-state emissive and substituent-tunable ph-sensitive bis-heterocyclic fluorescent probes, *J. Org. Chem.*, 2025, **90**, 5359-5371.
19. M. Olutas and A. Sagırlı, Solvatochromic and solid-state emissive azlactone-based AIEE-active organic dye: Synthesis, photophysical properties and color-conversion LED application, *J. Mol. Liq.*, 2020, **313**, 113482.
20. K. Li, Y. Zhu, B. Yao, Y. Chen, H. Deng, Q. Zhang, H. Zhan, Z. Xie and Y. Cheng, Rotation-restricted thermally activated delayed fluorescence compounds for efficient solution-processed OLEDs with EQEs of up to 24.3% and small roll-off, *Chem. Commun.*, 2020, **56**, 5957-5960.
21. D. Chowdhury, N. Hassan, S. Roy, M. D. H. Sanfui, P. Nandy, M. Chang, M. Rahaman, N. N. Ghosh, M. A. Hasnat, P. K. Chattopadhyay, D. K. Maiti and N. R. Singha, Exploring through-space charge transfer-mediated optoelectrochemical properties of dual-state luminescent aliphatic polymers and optoelectronic responses toward metal ions, *Langmuir*, 2024, **40**, 22265-22282.
22. B. Prusti and M. Chakravarty, Carbazole-anthranyl π-conjugates as small and stable aggregation-induced emission-active fluorogens: Serving as a reusable and efficient platform for anticounterfeiting applications with an acid key and multicolor ink for a quill pen, *ACS Omega*, 2019, **4**, 16963-16971.

23. Y. Xu, L. Ren, D. Dang, Y. Zhi, X. Wang and L. Meng, A strategy of "self-isolated enhanced emission" to achieve highly emissive dual-state emission for organic luminescent materials, *Chem. Eur. J.*, 2018, **24**, 10383-10389.
24. G. Bartwal, R. Manivannan, S. K. Patra and Y.-A. Son, A dual-state emissive TICT-AIEE-active near-infrared luminogen with multi-stimuli-responsive chromism for information display and data encryption, *Dyes Pigm.*, 2025, **240**, 112870.
25. Z. Ma, J. Tu, D. Yang, Q. Zhang and J. Wu, Recent advances in organic small-molecular dual-state emission probes, *J. Mol. Struct.*, 2024, **1312**, 138478.
26. Y. Liu, Y. Zhang, X. Wu, Q. Lan, C. Chen, S. Liu, Z. Chi, L. Jiang, X. Chen and J. Xu, Deep-blue luminescent compound that emits efficiently both in solution and solid state with considerable blue-shift upon aggregation, *J. Mater. Chem. C*, 2014, **2**, 1068-1075.
27. X. Zhang, Y. Zhou, M. Wang, Y. Chen, Y. Zhou, W. Gao, M. Liu, X. Huang and H. Wu, Metal-free facile synthesis of multisubstituted 1-aminoisoquinoline derivatives with dual-state emissions, *Chem. Asian J.*, 2020, **15**, 1692-1700.
28. W. Dai, P. Liu, S. Guo, Z. Liu, M. Wang, J. Shi, B. Tong, T. Liu, Z. Cai and Y. Dong, Triphenylquinoline (TPQ)-based dual-state emissive probe for cell imaging in multicellular tumor spheroids, *ACS Appl. Bio Mater.*, 2019, **2**, 3686-3692.
29. X. Mei, J. Wang, Z. Zhou, S. Wu, L. Huang, Z. Lin and Q. Ling, Diarylmaleic anhydrides: unusual organic luminescence, multi-stimuli response and photochromism, *J. Mater. Chem. C*, 2017, **5**, 2135-2141.
30. J. Wang, Z. Liu, S. Yang, Y. Lin, Z. Lin and Q. Ling, Large changes in fluorescent color and intensity of symmetrically substituted arylmaleimides caused by subtle structure modifications, *Chem. Eur. J.*, 2018, **24**, 322-326.
31. H. Wu, Z. Chen, W. Chi, A. K. Bindra, L. Gu, C. Qian, B. Wu, B. Yue, G. Liu, G. Yang, L. Zhu and Y. Zhao, Structural engineering of luminogens with high emission efficiency both in solution and in the solid state, *Angew. Chem., Int. Ed.*, 2019, **58**, 11419-11423.
32. Y. Zhang, Y. Qu, J. Wu, Y. Rui, Y. Gao and Y. Wu, Naphthalimide end-capping molecular rotors with different donor cores: Tuning emission in wide gamut and cell imaging, *Dyes Pigm.*, 2020, **179**, 108431.
33. N. Venkatramaiah, G. D. Kumar, Y. Chandrasekaran, R. Ganduri and S. Patil, Efficient blue and yellow organic light-emitting diodes enabled by aggregation-induced emission, *ACS Appl. Mater. Interfaces*, 2018, **10**, 3838-3847.
34. N. Jian, K. Qu, H. Gu, L. Zou, X. Liu, F. Hu, J. Xu, Y. Yu and B. Lu, Highly fluorescent triazolopyridine–thiophene D–A–D oligomers for efficient pH sensing both in solution and in the solid state, *Phys. Chem. Chem. Phys.*, 2019, **21**, 7174-7182.
35. P. Gopikrishna and P. K. Iyer, Monosubstituted dibenzofulvene-based luminogens: Aggregation-induced emission enhancement and dual-state emission, *J. Phys. Chem. C*, 2016, **120**, 26556-26568.
36. X. Zheng, W. Zhu, C. Zhang, Y. Zhang, C. Zhong, H. Li, G. Xie, X. Wang and C. Yang, Self-assembly of a highly emissive pure organic imine-based stack for electroluminescence and cell imaging, *J. Am. Chem. Soc.*, 2019, **141**, 4704-4710.
37. M. Mathivanan, B. Tharmalingam, C.-H. Lin, B. V. Pandiyan, V. Thiagarajan and B. Murugesapandian, ESIPT-active multi-color aggregation-induced emission features of triphenylamine–salicylaldehyde-based unsymmetrical azine family, *CrystEngComm*, 2020, **22**, 213-228.
38. C. Duan, Y. Zhou, G.-G. Shan, Y. Chen, W. Zhao, D. Yuan, L. Zeng, X. Huang and G. Niu, Bright solid-state red-emissive BODIPYs: facile synthesis and their high-contrast mechanochromic properties, *J. Mater. Chem. C*, 2019, **7**, 3471-3478.
39. N. Abid-Jarraya, K. Khemakhem, H. Turki-Guermazi, S. Abid, N. Saffon and S. Fery-Forgues, Solid-state fluorescence properties of small iminocoumarin derivatives and their analogues in the coumarin series, *Dyes Pigm.*, 2016, **132**, 177-184.
40. S. Ravi, S. Karthikeyan, M. Pannipara, A. G. Al-Sehemi, D. Moon and S. P. Anthony, Dual-state emission triphenylamine-coumarin fluorescent polymorphs: halochromic reversible fluorescence switching and π–π stacking facilitated picric acid sensing, *Mater. Adv.*, 2025, **6**, 3095-3103.
41. J.-M. Heo, J. Park, M. F. Flórez-Angarita, L. Wang, C. Yu, J. Choi, H. Woo, B. Milián-Medina, A. J. Matzger, M. S. Kwon, J. Gierschner and J. Kim, Elucidating the molecular structural origin of efficient emission across solid and solution phases of single benzene fluorophores, *Nat. Commun.*, 2025, **16**, 5560.
42. M. Durko-Maciag, G. Ulrich, D. Jacquemin, J. Mysliwiec and J. Massue, Solid-state emitters presenting a modular excited-state proton transfer (ESIPT) process: recent advances in dual-state emission and lasing applications, *Phys. Chem. Chem. Phys.*, 2023, **25**, 15085-15098.
43. H.-J. Son, W.-S. Han, K.-R. Wee, D.-H. Yoo, J.-H. Lee, S.-N. Kwon, J. Ko and S. O. Kang, Turning on fluorescent emission from C-alkylation on quinoxaline derivatives, *Org. Lett.*, 2008, **10**, 5401-5404.
44. H.-J. Son, W.-S. Han, D.-H. Yoo, K.-T. Min, S.-N. Kwon, J. Ko and S. O. Kang, Fluorescence control on panchromatic spectra via C-alkylation on arylated quinoxalines, *J. Org. Chem.*, 2009, **74**, 3175-3178.
45. P. Alam, N. L. C. Leung, H. Su, Z. Qiu, R. T. K. Kwok, J. W. Y. Lam and B. Z. Tang, A highly sensitive bimodal detection of amine vapours based on aggregation induced emission of 1,2-dihydroquinoxaline derivatives, *Chem. Eur. J.*, 2017, **23**, 14911-14917.
46. X. Huang, Z. Jiao, Z. Guo, J. Yang, P. Alam, Y. Liu, Y. Men, P. Zhang, H. Feng, S. Yao and B. Z. Tang, Development of reaction-based AIE handy pen for visual detection of toxic vapors, *ACS Mater. Lett.*, 2021, **3**, 249-254.
47. V. Dixit, A. Sharma, A. Jangid and N. Jain, Photo-induced functionalization of *para*-benzoquinones: access to dihydroquinoxalines with a tetrasubstituted carbon stereocenter., *Adv. Synth. Catal.*, 2023, **365**, 892-899.
48. T. K. Das, A. Ghosh, K. Balanna, P. Behera, R. G. Gonnade, U. K. Marelli, A. K. Das and A. T. Biju, N-Heterocyclic carbene-catalyzed umpolung of imines for the enantioselective synthesis of dihydroquinoxalines, *ACS Catal.*, 2019, **9**, 4065-4071.
49. T. H. Ho, B. K. Mai, T. A. To and T. V. Nguyen, A 1,2-aryl migration reaction in visible-light-mediated synthesis of quinoxaline derivatives: Mechanistic studies, *Org. Lett.*, 2024, **26**, 8842-8847.
50. T. Kumpulainen, B. Lang, A. Rosspeintner and E. Vauthey, Ultrafast elementary photochemical processes of organic molecules in liquid solution, *Chem. Rev.*, 2017, **117**, 10826-10939.
51. J. R. Lakowicz, *Principles of fluorescence spectroscopy*, Springer, New York, 2006.
52. E. Fresch and E. Collini, The role of h-bonds in the excited-state properties of multichromophoric systems: Static and dynamic aspects, *Molecules*, 2023, **28**, 3553.
53. A. Mukherjee, S. Bhattacharya and M. Chakravarty, An unprecedented pyridine-based dinuclear mixed-valent ReI/VII

View Article Online
DOI: 10.1039/D6QM00234J

oxo-bridged complex: a solvatochromic and AIE-active probe for nanomolar detection of picric acid and trinitrotoluene, *Dalton Trans.*, 2021, **50**, 9144-9157.
54. C. Reichardt, Solvatochromic dyes as solvent polarity indicators, *Chem. Rev.*, 1994, **94**, 2319-2358.
55. C. S. Abeywickrama, Large Stokes shift benzothiazolium cyanine dyes with improved intramolecular charge transfer (ICT) for cell imaging applications, *Chem. Commun.*, 2022, **58**, 9855-9869.
56. B. Valeur and M. N. Berberan-Santos, *Molecular fluorescence: principles and applications*, Wiley-VCH Verlag GmbH & Co. KGaA, Weinheim, 2013.
57. P. Sahu, S. I. Islam, R. K. Mitra and D. K. Palit, A complete description of the ultrafast proton transfer dynamics in the excited state of d-luciferin, *The Journal of Physical Chemistry B*, 2025, **129**, 1046-1060.
58. A. Guijarro, J. A. Vergés, E. San-Fabián, G. Chiappe and E. Louis, Herringbone pattern and CH–π bonding in the crystal architecture of linear polycyclic aromatic hydrocarbons, *ChemPhysChem*, 2016, **17**, 3548-3557.
59. G. R. Desiraju, Hydrogen bridges in crystal engineering: Interactions without borders, *Acc. Chem. Res.*, 2002, **35**, 565-573.
60. C. A. Hunter and J. K. M. Sanders, The nature of .pi.-.pi. interactions, *J. Am. Chem. Soc.*, 1990, **112**, 5525-5534.
61. L. Zou, S. Guo, H. Lv, F. Chen, L. Wei, Y. Gong, Y. Liu and C. Wei, Molecular design for organic luminogens with efficient emission in solution and solid-state, *Dyes Pigm.*, 2022, **198**, 109958.
62. G. R. Fulmer, A. J. M. Miller, N. H. Sherden, H. E. Gottlieb, A. Nudelman, B. M. Stoltz, J. E. Bercaw and K. I. Goldberg, NMR chemical shifts of trace impurities: Common laboratory solvents, organics, and gases in deuterated solvents relevant to the organometallic chemist, *Organometallics*, 2010, **29**, 2176-2179.
63. M. J. Frisch, G. W. Trucks, H. B. Schlegel, G. E. Scuseria, M. A. Robb, J. R. Cheeseman, G. Scalmani, V. Barone, G. A. Petersson, H. Nakatsuji, M. C. X. Li, A. V. Marenich, J. Bloino, B. G. Janesko, R. Gomperts, B. Mennucci, H. P. Hratchian, J. V. Ortiz, A. F. Izmaylov, J. L. Sonnenberg, F. D. Williams, F. Lipparini, F. Egidi, J. Goings, B. Peng, A. Petrone, T. Henderson, D. Ranasinghe, V. G. Zakrzewski, J. Gao, N. Rega, G. Zheng, W. Liang, M. Hada, M. Ehara, K. Toyota, R. Fukuda, J. Hasegawa and T. N. M. Ishida, Y. Honda, O. Kitao, H. Nakai, T. Vreven, K. Throssell, J. A. Montgomery Jr., J. E. Peralta, F. Ogliaro, M. J. Bearpark, J. J. Heyd, E. N. Brothers, K. N. Kudin, V. N. Staroverov, T. A. Keith, R. Kobayashi, J. Normand, K. Raghavachari, A. P. Rendell, J. C. Burant, S. S. Iyengar, J. Tomasi, M. Cossi, J. M. Millam, M. Klene, C. Adamo, R. Cammi, J. W. Ochterski, R. L. Martin, K. Morokuma, O. Farkas, J. B. Foresman and D. J. Fox, 2016, Gaussian 16 Rev. C.01, Wallingford, CT.
64. T. Yanai, D. P. Tew and N. C. Handy, A new hybrid exchange–correlation functional using the Coulomb-attenuating method (CAM-B3LYP), *Chem. Phys. Lett.*, 2004, **393**, 51-57.
65. F. Weigend and R. Ahlrichs, Balanced basis sets of split valence, triple zeta valence and quadruple zeta valence quality for H to Rn: Design and assessment of accuracy, *Phys. Chem. Chem. Phys.*, 2005, **7**, 3297-3305.
66. J.-D. Chai and M. Head-Gordon, Long-range corrected hybrid density functionals with damped atom–atom dispersion corrections, *Phys. Chem. Chem. Phys.*, 2008, **10**, 6615-6620.
67. W. Kabsch, A solution for the best rotation to relate two sets of vectors, *Acta Cryst. A.*, 1976, **32**, 922-923.